Small Molecule Photoelectron Spectroscopy: Recoil Effects, Stoichiometric Surprises, and Double-Core-Hole Ionization

T. Darrah Thomas

Department of Chemistry, Oregon State University, Corvallis, OR 97330, USA

Abstract

Three features of small-molecule photoelectron spectroscopy are considered (1) The atom from which a photoelectron is emitted must have a recoil momentum equal to that of the emitted electron. This is shared among the various modes of motion of the ion, leading to rotational and vibrational excitation. Furthermore, any initial velocity of the atom (due to either translational, rotational, or vibrational motion) will lead to Doppler broadening. These effects are observable and can, in general, be accounted for by simple models. In some cases, however, the simple models fail and a deeper insight is necessary. (2) Inner-shell photoionization is essentially an atomic process, and it is expected that the intensity for emission of a photoelectron from the core of an atom in a molecule will be independent of its chemical environment. Recent measurements on the carbon 1s photoelectron spectra of three chloroethanes show that this is not the case. At energies not far above the ionization threshold there are strong oscillations of the intensity ratio (C_{Cl}/C_H) with increasing photon energy. These are similar to those seen in EXAFS and can be accounted for by considering backscattering of the photoelectrons from the chlorine atoms. Moreover, even at high energies the cross section for ionization has been found to depend on the chemical environment of the atom. These results have important consequences for the use of inner-shell electron spectroscopy for quantitative analysis. (3) Single-core-hole ionization energies have long been used as a tool for investigating chemical phenomena. Double-core-hole ionization energies provide additional chemical information. By combining the single-hole and double-hole ionization energies it is possible to determine the effects of the initial-state charge distribution and final-state charge rearrangement on the chemical shifts and on other chemical properties. Until recently double-core-hole ionization energies have not been experimentally accessible for first-row elements. New experimental techniques have, however, made it possible to measure these not only for single sites in a molecule, but also for two different sites in the same molecule. The chemical information that can be obtained from such measurements is discussed.

Keywords: inner-shell ionization, recoil excitation, photoelectron intensities, double-core-holes

1. Introduction

For more than 40 years, photoelectron spectroscopy has proved to be an important tool for studying a variety of phenomena in atoms, molecules, surfaces, and solids. As its name implies, the technique involves an incident photon and an ejected electron, whose kinetic energy is measured. For inner-shell photoelectron spectroscopy the kinetic energy reflects the elemental identity of the atom from which the electron is ejected, and, in more detail, it reflects the chemical environment of the atom. The intensity of a particular photoelectron peak in the spectrum depends on the number of atoms of that particular kind that are in the sample, but recent experiments [1] show that the intensities can differ markedly from those expected from the stoichiometry of the molecule. Relevant results are described in Sect. 3.

The chemical shifts of the kinetic energies between photoelectrons from the same element in different environments are well known and have long been exploited to provide insights into chemical properties and as an analytical tool to identify the chemical nature of a particular atom. Additional chemical information can be obtained if the one-hole ionization energies that are obtained in conventional photoelectron spectroscopy can be compared with measurements of two-hole ionization energies. Until recently, two-hole ionization energies were available only via core-core-core Auger spec-

troscopy, precluding the possibility of measurements of these quantities for first-row elements. Recently, however, new experimental techniques have opened up the possibility for such measurements in first-row elements. Some of the implications and opportunities of this newly acquired ability have been discussed in refs. [2, 3] and are reviewed briefly in Sect. 4.

For ionization of an atom that is initially at rest the photon energy, $h\nu$, must be equal to the sum of the ionization energy, I, and the total kinetic energy, ϵ_{kin}, of the photoelectron and the ion. The total kinetic energy divides between the two particles according to conservation of momentum, with the consequence that each receives a kinetic energy that is proportional to the mass of the partner fragment. Thus we have

$$h\nu = I + \epsilon_{kin} = I + \epsilon_e + \epsilon_{ion} \tag{1}$$

$$= I + \epsilon_{kin}M_{ion}/M_A + \epsilon_{kin}m_e/M_A \tag{2}$$

where ϵ_e and ϵ_{ion} are the kinetic energies of the electron and the ion. M_A, M_{ion}, and m_e are the masses of the atom, ion, and electron. Since $M_A \approx M_{ion}$ and $m_e << M_A$, the electron kinetic energy is almost equal to the total kinetic energy and the ion kinetic energy (often referred to as the "recoil" energy) is small.

If the electron is ionized from an atom in a molecule, then conservation of momentum applies to both the atom and the molecule. The recoil energy for the atom is equal to $\epsilon_e m_e/M_A$, whereas that for the molecule is less, $\epsilon_e m_e/M_M$, where M_M is the mass of the molecule. The difference between these appears as internal excitation of the molecular ion – vibrational and rotational – and thus we have what may be referred to as "recoil-induced" vibrational and rotational excitation of the ion [4]. Although such effects were predicted theoretically many years ago [5], they have been observed experimentally only in the last few years [6–11].

In addition to the recoil effects just mentioned, the final energies of both the electron and the ion are affected by any initial kinetic energy that the atom may have. This appears as a Doppler broadening of the spectral lines. Doppler broadening due to translational motion is quite familiar, but in addition there can be broadening arising from the kinetic energy that the atom may have as a result of the rotational or vibrational motion of the molecule. Rotational Doppler broadening in molecular systems was predicted theoretically only recently [12] and observed experimentally only in 2011 [13]. The various recoil effects are discussed in more detail in section 2.

2. Recoil effects

The difference, ΔE, between the recoil energy of the atom from which the electron is ejected and that of the molecular ion is equal to $\epsilon_e m_e \left(1/M_A - 1/M_M\right)$. This energy goes into internal (rotational and vibrational) excitation of the molecular ion. The division of this energy among the various normal modes of the ion depends on the direction of emission of the electron with respect to the molecular frame, on the location of the atom from which the electron is emitted in the ion, and on the normal-mode vectors of the ion [7]. For isotropic emission from a diatomic molecule one-third of the recoil excitation energy goes into vibrational excitation and two-thirds into rotational excitation. If the atom from which the electron is emitted is at the center of mass of the molecule (as in carbon 1s ionization of CH_4 and CF_4), then there is only vibrational excitation. Specific examples of recoil-induced rotational and vibrational excitation are discussed in the following sections.

2.1. Rotational effects

For most photoelectron spectroscopic measurements it is not possible to resolve the individual rotational states of the final ion. It is, therefore, necessary to consider the average effect of the recoil-induced rotational excitation. For this purpose, a classical model is sufficient to account for the features observed in currently available data. For emission of an electron with momentum k from atom A of a linear molecule, the change in rotational energy due to the recoil is given by the following expression [8, 10].

$$\Delta E_{rot} = (k^2 R_A^2 \sin^2\theta - 2kJ_0 R_A \sin\theta \cos\phi)/(2I) \tag{3}$$

R_A is the distance of atom A from the center of mass of the molecule, J_0 is the initial angular momentum of the molecule, and I the moment of inertia of the molecule [14]; θ and ϕ define the direction of emission with respect to the molecular frame. To average over the angles of emission it is necessary to know the angular distribution of the photoelectrons in the molecular framework. For a linear molecule this depends only on θ, and the normalized angular distribution $P(\theta)$ can be expressed as

$$P(\theta) = \sum_k A_k P_k(\theta)/2A_0 \tag{4}$$

$P_K(\theta)$ is a Legendre polynomial and the A_k's are coefficients that describe the angular distribution. Combining eqs. 3 and 4 and averaging over θ and ϕ gives

$$\langle \Delta E_{rot} \rangle = \left(\frac{2}{3} - \frac{A_2}{A_0} \frac{4}{15} \right) \frac{R_A^2 k^2}{2I} \tag{5}$$

2

For a diatomic molecule eq. 5 becomes

$$\langle \Delta E_{rot} \rangle = \left(\frac{2}{3} - \frac{A_2}{A_0} \frac{4}{15} \right) \epsilon_e m_e \left(\frac{1}{M_a} - \frac{1}{M_m} \right) \quad (6)$$

For an isotropic distribution ($A_2 = 0$), the factor represented by the first set of parentheses is 2/3. If $P(\theta) \propto sin^2\theta$, it is 4/5, and if $P(\theta) \propto cos^2\theta$ it is 2/5.

2.1.1. Rotational-recoil-induced shifts

Eq. 6 shows that the average rotational energy and, hence, the apparent ionization energy, increases linearly with the kinetic energy of the outgoing electron. The slope of the increase depends on the molecular-frame angular distribution of the photoelectrons. The apparent ionization energy can be measured from spectra such as shown in Fig. 1, which shows the valence photoelectron spectrum of a mixture of N_2 and Kr. The Kr, for which the ionization energy is well known, provides a reference line for both the energy scale and the resolution. The difference in positions between the N_2 peaks and the Kr peaks can be measured with an accuracy of about 1 meV, and consequently the apparent ionization energy of N_2 can be measured with similar accuracy.
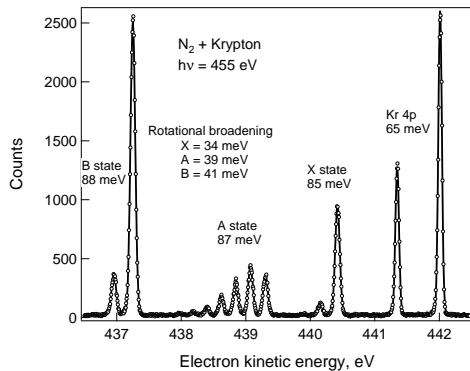
Figure 1: Valence photoelectron spectrum of a mixture of N_2 and Kr at a photon energy of 455 eV. The numbers indicated for each group of peaks show the width of the peak (FWHM). The numbers indicated as "rotational broadening" show the widths corrected for instrumental and translational Doppler broadening. Data from [15].

The expected linear increase of the apparent ionization energy can be seen in Fig. 2, where the energy of the $B^2\Sigma_u^+$ state of N_2^+ (relative to that of the ground state of N_2) is plotted versus the kinetic energy of the outgoing electron. The solid line, with a slope of 1.31×10^{-5}, shows the prediction based on eq. 6 assuming that the photoelectron emission is isotropic in the molecular frame. Isotropic emission is expected, since the ejected electron comes from a molecular orbital that has primarily nitrogen $2s$ character. The prediction is in good

agreement with the experimental results. Also shown in the figure as the dashed line is the prediction of a quantum mechanical model that takes into account interference between the emission from one of the nitrogen atoms and that from the other. The oscillatory behavior results from the alternating constructive and destructive nature of this interference. Unfortunately the currently available data are not good enough to verify this prediction.
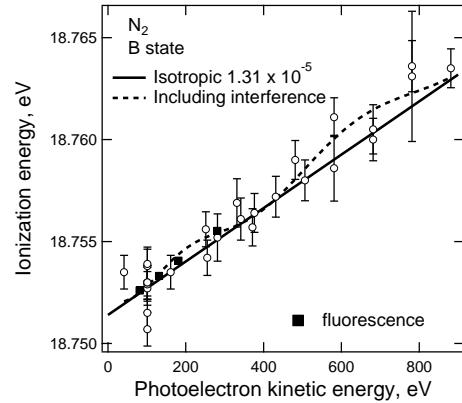
Figure 2: Apparent ionization energy to produce the $v = 0$ B state of N_2^+ as a function of photoelectron kinetic energy. Circles are based on photoelectron spectroscopic measurements and squares on rotationally resolved fluorescence measurements. The solid line shows the behavior predicted by eq. 6 assuming isotropic emission. The dashed line shows the predictions of a quantum mechanical model. See refs. [8, 10] for additional details.

Similar results to those shown in Fig. 2 are observed for ionization to produce the X and A states of N_2^+ and the X, A, and B states of CO^+ [10]. In the simplest approximation the photoelectron emission is expected to be isotropic in the molecular frame for the B state of N_2^+ and we see in Fig. 2 that the prediction based on this assumption is in good agreement with the experimental results. For the X state, however, which has primarily nitrogen $2p_\sigma$ character, we expect a photoelectron distribution that goes as $cos^2\theta$, and, therefore a lower slope. The A state has exclusively nitrogen $2p_\pi$ character, and, consequently an angular distribution that goes as $sin^2\theta$, and a higher slope. The slopes obtained from fitting the experimental data are summarized in Table 1, where they are compared with these predicted slopes. There is approximate but not quantitative agreement between the predictions and the measurements, indicating that the picture drawn here is too simple. As an example, it can be noted that for the X state, the orbital in question is not pure $2p_\sigma$ but contains some admixture of $2s$, leading to an angular distribution somewhere be-

tween $cos^2\theta$ and isotropic and, hence, to a higher slope than predicted. Further discussion of this question can be found in ref. [10]. It is, however, apparent that the amount of recoil-induced rotational excitation depends on the symmetry of the molecular orbital and, consequently, on the molecular-frame angular distribution of the photoelectron.

Table 1: Slopes of the lines representing the dependence of apparent ionization on electron kinetic energy for the valence state of N_2^+. From ref. [10].

State	Type	$P(\theta)$	Measured 10^{-5}	Predicted 10^{-5}
X	$2p_\sigma$	$cos^2\theta$	1.00 ± 0.06	0.78
A	$2p_\pi$	$sin^2\theta$	1.40 ± 0.12	1.57
B	$2s$	isotropic	1.40 ± 0.08	1.31

2.1.2. Rotational Doppler broadening

In Fig. 1 the numbers associated with each group of peaks indicate the measured widths of the peaks (FWHM). These arise from both instrumental and Doppler broadening. The widths for the N_2 peaks are broader than those for the Kr reference peak, even though the instrumental broadening is the same for both N_2 and Kr. This difference arises from differences in the Doppler broadening. Part arises because the mass of Kr is greater than the mass of N_2, but even after correcting for this, there is a residual difference, shown in Fig. 1. This is due to rotational Doppler broadening arising from the kinetic energy that the nitrogen atoms have because the molecule is rotating. This effect was predicted by Sun et al. [12] and verified experimentally by Thomas et al. [13].

The Doppler broadening, σ_D, can be found from the variance of the distribution of the recoil energies, ϵ_{ion}, or electron energies, ϵ_e.

$$\sigma_D^2 = \left\langle \epsilon_{e,ion}^2 \right\rangle - \left\langle \epsilon_{e,ion} \right\rangle^2. \tag{7}$$

For emission from an atom with an initial kinetic energy of ϵ_0

$$\sigma_D^2 = (4/3)(m_e/M_A)\epsilon_0\epsilon_e \tag{8}$$

For a free atom in the gas phase at temperature T the average value of the initial energy is $3k_BT/2$, where k_B is the Boltzmann constant. Then we have that

$$\sigma_{D,trans}^2 = 2(m_e/M_A)k_BT\epsilon_e \approx 2\epsilon_{ion}k_BT \tag{9}$$

which is the usual expression for translational Doppler broadening.

Starting with eq. 6 for ΔE_{rot} we can derive a similar expression for rotational Doppler broadening,

$$\begin{aligned}
\sigma_{D,rot}^2 &= \left\langle \Delta E_{rot}^2 \right\rangle - \left\langle \Delta E_{rot} \right\rangle^2 \\
&\approx 2\left\langle \Delta E_{rot} \right\rangle J_0^2/(2I) \tag{10} \\
&= 2\left\langle \Delta E_{rot} \right\rangle kT_B \tag{11}
\end{aligned}$$

Eq. 11 results from averaging over the initial values of J_0 [16]. The expressions for the rotational Doppler broadening, 10 and 11, are very similar to those for translational Doppler broadening, 8 and 9.

We see from eq. 11 that the variance of the distribution, which reflects the rotational Doppler broadening, is proportional to the recoil-induced shifts in the apparent ionization energy, ΔE_{rot}. Since ΔE_{rot} increases linearly with the photoelectron kinetic energy, the variance also increases linearly with this energy. This behavior can be seen in Fig. 3, where the variance has been plotted against the electron kinetic energy. The dotted line

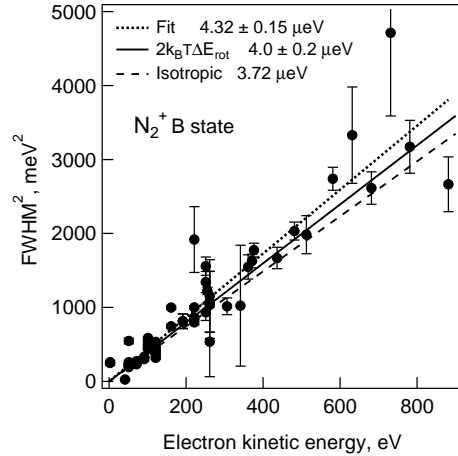Figure 3: Rotational contribution to the width of the B-state peaks in the N_2 photoelectron spectrum. The square of the width (FWHM) is plotted against the photoelectron energy. The dotted line shows a fit of a straight line to the data. The solid line shows the prediction based on eq. 11. The dashed line shows the prediction for isotropic emission of the photoelectron. The values are the slopes of the lines. Data from ref. [13].

in Fig. 3 shows the fit of a straight line to the data. The solid line is obtained using eq. 11 and the empirically observed slope (1.4×10^{-5}, see Table 1) for the relationship between ΔE_{rot} and the electron kinetic energy together with the room-temperature value of kT_B. The dashed curve uses the theoretical value of 1.3×10^{-5} for the slope (obtained from eq. 6 assuming isotropic emission). The parameters of the three lines are similar, indicating agreement between observation and prediction for the rotational Doppler broadening.

The temperature dependence implicit in eq. 11 has been verified from low-temperature data [13, 17].

Comparing eqs. 9 and 11 we see that the ratio of the variances for the two types of Doppler broadening are given by the relationship

$$\sigma_{D,rot}^2 / \sigma_{D,trans}^2 = \Delta E_{rot}/\epsilon_{ion} \tag{12}$$

The two energies, ΔE_{rot} and ϵ_{ion}, are comparable, and, as a consequence the rotational and translational Doppler broadening can be comparable. For instance, in a typical experiment of the type illustrated in Fig. 1 the translational Doppler broadening is 52 meV and the rotational Doppler broadening is 45 meV [13]. In many cases it is the Doppler broadening that sets the limit on the instrumental resolution and it is, therefore, important to assess the rotational contribution to this broadening in each case.

2.2. Vibrational effects

Although recoil-induced vibrational excitation was predicted by Domcke and Cederbaum in 1978 [5], it was not observed experimentally until 2005 by Kukk et al. [6], who found evidence for it in the carbon 1s photoelectron spectrum of CH_4. More striking evidence was seen in 2008 in the carbon 1s photoelectron spectrum of CF_4 [7]. For these molecules the ionization takes place at the center of mass of the molecule, with the result that there is no recoil-induced rotational excitation. Furthermore, the normal Franck-Condon vibrational excitation, which results from differences in the geometries of the neutral and ionized molecules [18], gives rise to excitation of only the symmetric vibrational modes, whereas the recoil-induced vibrational excitation leads to excitation of the asymmetric modes. In addition, for CF_4 there is only weak Franck-Condon excitation and the intrinsic (lifetime) width for the carbon 1s core hole is exceptionally narrow. These features combine to make CF_4 an ideal candidate for observing recoil-induced vibrational excitation.

High-resolution photoelectron spectra generally show resolved vibrational structure. Accordingly it is necessary to use a quantum-mechanical model to describe the vibrational profile. This is conveniently done using a harmonic oscillator model. In dimensionless units the energy is measured in units of $\hbar\omega$, and the momentum and position coordinates p and q are given by the expressions

$$p = p'/\sqrt{\hbar\mu\omega} \quad \text{and} \quad q = x\sqrt{\mu\omega/\hbar} \tag{13}$$

where p' is the momentum in real space, x is the distance coordinate in real space, μ is the reduced mass, and ω is the characteristic frequency of the oscillator. We can work in either position or momentum coordinates. The corresponding Hamiltonians are

$$\hat{H}_q = -\frac{1}{2}\frac{\partial^2}{\partial q^2} + \frac{q^2}{2} \quad \text{and} \quad \hat{H}_p = -\frac{1}{2}\frac{\partial^2}{\partial p^2} + \frac{p^2}{2} \tag{14}$$

Because of the symmetry of the Hamiltonians in p and q the wave functions in momentum space are identical in form to those in distance space.

If the initial molecule is in its vibrational ground state and the vibrational frequencies for the ion are the same as the vibrational frequencies for the neutral molecule, then the Franck-Condon factors, $|\langle 0|v\rangle|^2$, follow a Poisson distribution:

$$|\langle 0|v\rangle|^2 = \frac{S^v}{v!}\exp(-S) \tag{15}$$

with $S = \delta q^2/2$ or $S = \delta p^2/2$, depending on whether we are working in position or momentum coordinates. The quantities δp and δq are, respectively, the change in the normal coordinate of the vibrational mode of interest or the additional momentum added to the motion in this coordinate because of the emission of the photoelectron. A detailed discussion of these expressions and of the methods for dividing the recoil momentum among the normal modes is found in ref. [7].

For the Poisson distribution S is equal to the average value of v, and, hence, the average excitation energy is $S\hbar\omega$. For recoil-induced vibrational excitation the average vibrational excitation energy can be shown to be proportional to the kinetic energy of the photoelectron [7]. S is also equal to the ratio of the intensity of the $v = 1$ peak in the photoelectron spectrum to that of the $v = 0$ peak. Hence, this ratio should also vary linearly with the photoelectron kinetic energy.

As noted above, CF_4 provides a particularly useful example of recoil-induced vibrational excitation. Carbon 1s photoelectron spectra measured at photon energies of 330 eV, 800 eV, and 1500 eV are shown in Fig. 4. At the lowest energy the peak is slightly asymmetric because of post-collision interaction and has a weak contribution from the the $v = 1$ excitation of the symmetric stretching mode. At this energy there is no observable contribution from recoil. At 800 eV there is no post-collision interaction, and, therefore, we expect symmetric peaks. However, a pronounced asymmetry is apparent in the spectrum, and this is due to the recoil-induced excitation of the asymmetric stretching mode. At 1500 eV this contribution is even more pronounced. From these spectra it is possible to extract the $(v = 1)/(v = 0)$ intensity ratio for the excitation of the asymmetric stretching mode.
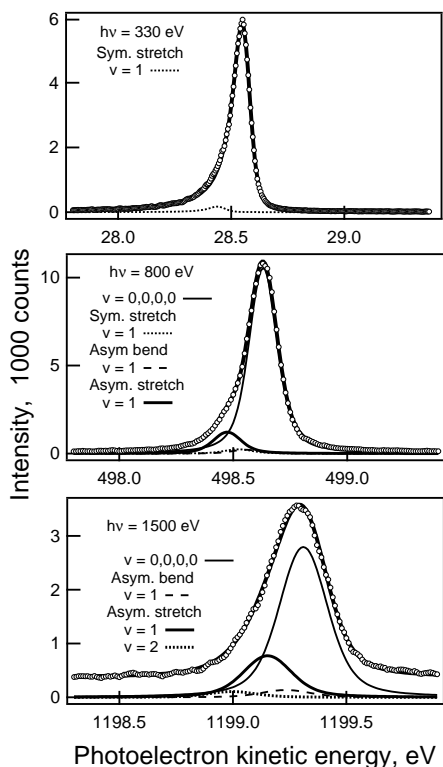
5

Figure 4: Carbon 1s photoelectron spectra of CF_4 at three photon energies. The open circles show the data. The lines represent the contributions of various vibrational states to the spectrum as well as the sum of these individual contributions. Data from ref. [7].

Figure 5: Intensity ratio $(v = 1)/(v = 0)$ for the asymmetric stretching mode in the C 1s photoelectron spectrum of CF_4. Plotted against the photoelectron kinetic energy. Points are experimental results and the solid line is a theoretical prediction with no adjustable parameters.

The dependence of the intensity ratio on the photoelectron kinetic energy is shown in Fig. 5, where the linearity is readily apparent. The solid line in this figure shows the predictions of theory, with no adjustable parameters. The agreement is excellent.

There will also be Doppler broadening associated with the vibrational motion. At low temperatures where the neutral molecule is in its vibrational ground state, this effect is already included in eq. 15. In this case $\sigma_{D,vib}^2 = S(\hbar\omega)^2 = \Delta E_{vib}\hbar\omega$, where ΔE_{vib} is the recoil-induced vibrational excitation. In the high-temperature limit $\sigma_{D,vib}^2 = 2kT_B\Delta E_{vib}$, identical to the translational Doppler broadening, eq. 9. The transition between these two limits has been explored by Fujikawa et al. [19].

2.3. Some puzzles

The examples discussed above show good agreement between what is observed and what is expected. This is not always the case, as illustrated by two examples discussed below. A third example shows results t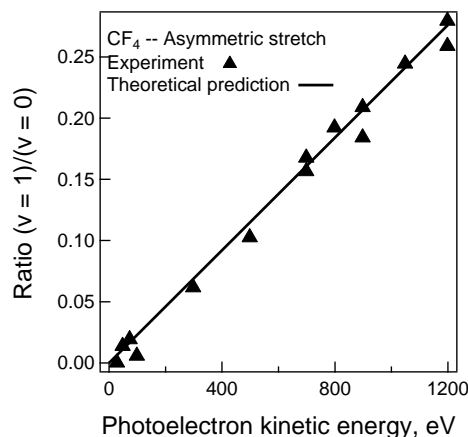hat may be reasonable but are not included in the models considered above. In all of these cases further experimental work is needed.

2.3.1. Carbon 1s ionization in CO

In Fig 6 the $(v = 1)/(v = 0)$ intensity ratio for carbon 1s ionization of CO is plotted against the photon energy. This case differs from that shown above for CF_4 in that there is strong Franck-Condon excitation of the v=1 vibrational state even in the absence of any recoil-induced excitation. Included in this figure are previously published results (open points) [20, 21] at low energy together with results spanning a wider energy range (solid points, unpublished results from MAX II and SPring-8 by the authors of refs. [7, 8, 10]). There is good agreement between the recent measurements and the previously published results in the region where there is overlap.

At low photon energies the intensity ratio is strongly influenced by near-threshold effects [21]. At higher energies, however, we expect a constant ratio from normal Franck-Condon excitation plus an increasing contribution from recoil-induced excitation. The predicted behavior for isotropic emission of the carbon 1s photoelectron is shown as the dashed line, which has been normalized to the experimental point at a photon energy of 600 eV. More detailed calculations by Plésiat et al. [22] also predict an overall increase in the ratio for photon energies above about 700 eV. The data do not follow these predictions. To the contrary the trend line for the data above 500 eV (solid line in Fig. 6) shows that the ratio decreases with increasing photon energy [23].

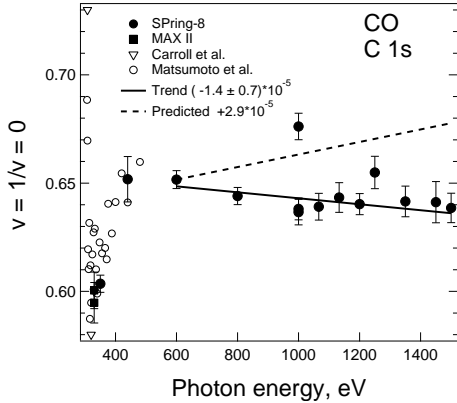At this point, we can only speculate on the source

6

Figure 6: Intensity ratio, $(v = 1)/(v = 0)$, for carbon 1s ionization of CO, plotted against photon energy. The open points are from refs. [20, 21] and the closed points are from unpublished results by the authors of refs. [7, 8, 10]. The solid line shows a fit of a straight line to the data at photon energies above 500 eV. The dashed line shows the prediction for isotropic emission, normalized to the point at 600 eV.

of this disagreement. One possibility is that the angular distribution of the photoelectrons is strongly peaked in the direction perpendicular to the molecular axis, resulting in recoil-induced vibrational excitation weaker than predicted. This would not lead to a decreasing ratio. Another possibility is that there is interference between the two types of vibrational excitation. We can guess (without justification) that the combined effects of normal Franck-Condon excitation and recoil-induced excitation can be obtained by setting S in eq. 15 equal to $\left|\delta q + \delta p e^{i\phi}\right|^2 /2$, where δq represents the contribution from geometric changes, δp that from momentum changes, and ϕ any phase shift between the two amplitudes. Then there is the possibility of destructive interference between the two contributions, leading to the observed negative slope in Fig. 6. Whether such an effect exists is uncertain. According to Domcke and Cederbaum [5] "there is a complicated interference between the internal [Franck-Condon] and the recoil-induced contributions to the vibrational intensity distribution". On the other hand, the generalized Franck-Condon factors discussed by Ueda et al. [24] yield $\phi = \pi/2$ and $S = (\delta q^2 + \delta p^2)/2$, that is that there is no interference and that the overall vibrational intensity distribution is simply the convolution of the two distributions. This is currently a subject of ongoing experimental and theoretical investigation [25, 26].

2.3.2. Polarization dependence in the valence photoelectron spectrum of N_2

For most of our measurements a single polarization of the photon beam was used throughout the series of experiments. For the valence photoelectron spectra of N_2 we have a few measurements in which the polarization was varied [15]. One set of these involves the $(v = 1)/(v = 0)$ intensity ratios for the X and B states of N_2^+, measured for three different angles, γ, ($0°$, $54.7°$, and $90°$) between the polarization direction and the electron propagation direction and two different photon energies, 70 and 240 eV. The intensity ratios determined in these experiments are summarized in Table 2. The quantities listed in this table are a ratio of ratios, that is, the ratio $(v = 1)/(v = 0)_\gamma$ divided by the ratio $(v = 1)/(v = 0)_{54.7}$. At a photon energy of 70 eV vi-

Table 2: Dependence of the vibrational excitation in the valence photoelectron spectrum of N_2 on polarization and photon energy. $((v = 1/v = 0)_\gamma/(v = 1/v = 0)_{54.7})$

Photon energy (eV)		70		240	
State		X	B	X	B
$\gamma =$ 54.7°		1	1	1	1
0°		0.97	0.86	1.06	1.13
90°		1.08	1.09	0.98	1.04

brational excitation appears to be enhanced for 90° polarization and suppressed for 0° polarization. At 240 eV we see the reverse effect. The results given in Table 2 are equivalent to the observation that the angular anisotropy parameter β depends on both the vibrational quantum number and the photon energy. A dependence of β on photon energy is known for many systems and a dependence on vibrational quantum number is known in a few cases, primarily associated with shape resonances [27–29]. In the present case we are well above the region of the shape resonance and we do not have an explanation for either the enhancement or the reversal. We note however that the Cooper minimum in N_2 occurs between these two energies [30] and speculate that the reversal might arise from an interference effect associated with the change in sign of the matrix element at the minimum. Alternatively, these effects might arise from Cohen-Fano interference [31], and a number of reports [24, 32, 33] have noted that such interference has a noticeable effect on the vibrational intensities observed in both valence and core photoionization. These explanations are possibly related, as noted by López-Dominguez et al. [34], who have recently discussed the effect of the Cooper minimum on vibrational profiles in the valence photoionization of N_2 and CO and have

pointed out the connection between the Cooper minimum and Cohen-Fano oscillations.

Another effect of polarization is seen if we consider the rotational excitation. This is illustrated in Table 3, where the results for recoil-induced rotational excitation and the rotational Doppler broadening for photoionization to form the X state of N_2^+ at a photon energy of 70 eV are summarized. Also shown here are the data for vibrational excitation, taken from Table 2.

Table 3: Dependence of the rotational and vibrational excitation on polarization for the X state in N_2^+ at a photon energy of 70 eV.

γ	Rotational^a	Rot. Dop.^{b}	Vibrational^c
54.7	0	1	1
90	1.0	1.63	0.97
0	-0.5	0.64	1.08

a. $\Delta E_{rot,\gamma} - \Delta E_{rot,54.7}$, meV
b. $\sigma_\gamma^2/\sigma_{54.7}^2$
c. $(v = 1/v = 0)_\gamma/(v = 1/v = 0)_{54.7}$

These results show that if the polarization direction coincides with the electron propagation direction ($0°$) then there is slightly less rotational excitation and Doppler broadening and slightly more vibrational excitation than at $54.7°$. Conversely, at $90°$ there is more rotational excitation and rotational Doppler broadening and less vibrational excitation. These results can be accounted for by a picture in which ionization occurs preferentially when the axis of the molecule is aligned with the polarization direction. In this case, γ, the polarization direction, and θ, the direction of the electron with respect to the molecular axis, coincide. For $\theta \approx \gamma = 0°$, there will be enhancement of vibrational excitation, since the recoil momentum will be along the molecular axis. For $\theta \approx \gamma = 90°$, rotational excitation will be enhanced.

The X state of N_2^+ is a Σ state as is the B state. Similar results to those seen in Table 3 are also seen for the B state. By contrast, the A state, which has Π symmetry, shows the reverse effect. These results suggest that there is a preference for ionization for particular orientations of the molecule with respect to the polarization direction and that this preference depends on the symmetry of the ionized orbital.

3. Stochiometric surprises

Inner-shell ionization of atoms in molecules is expected to be essentially an atomic process. Even though inner-shell ionization energies depend on the chemical environment, these energy shifts arise primarily from interaction of the inner-shell atomic orbitals with the surroundings and not from differences in the orbitals themselves. Thus we might expect that the *probability* for ionization, which involves the matrix element between the atomic orbital and the outgoing electron, would be independent of the chemical environment. This expectation has been the basis of the use of inner-shell electron spectroscopy as a tool for quantitative analysis. Recent results [1] show, however, that the relative intensities in inner-shell photoelectron spectra can differ markedly from those expected from the stoichiometry of the molecule.
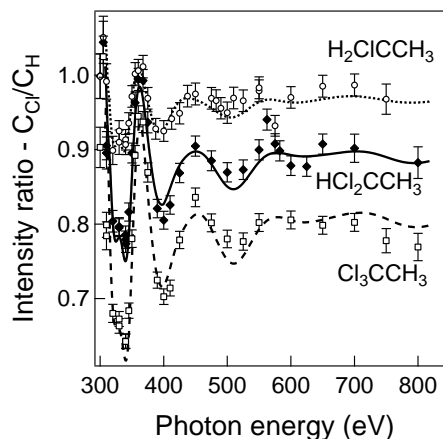
Figure 7: The C_{Cl}/C_H intensity ratio for chloroethanes. The points show experimental measurements and the lines show theoretical predictions based on EXAFS-type calculations. From ref. [1]

Fig. 7 shows typical results for the carbon 1s photoelectron spectra of chloroethanes, $CH_3CH_{3-n}Cl_n$ $n = 1, 2, 3$, where the intensity ratio C_{Cl}/C_H is plotted against the photon energy [1]. From the stoichiometry of the molecules we might expect this ratio to be equal to 1 and independent of the photon energy. To the contrary, we see that the ratio can be significantly less than 1, that it oscillates with photon energy, and reaches an asymptotic value of less than 1. The oscillations can be understood as arising primarily from interference between the outgoing photoelectrons and those that are backscattered from the chlorine atoms. The curves, which are based on such a backscattering model, account well for the oscillations. The effect increases with the number of chlorine atoms. In addition to this effect, the intensity for the chlorinated carbon atoms is reduced by the effects of inelastic processes that are enhanced by the nearby chlorine atoms, such as shake-up/off and internal inelastic scattering. Further

discussion can be found in ref. [1].

The examples shown in Fig. 7 are not unusual, and we have observed many similar cases. Some of these are summarized in Table 4, which shows intensity ratios for carbon 1s photoionization measured at a photon energy of 330 eV for a number of systems.

Table 4: Intensity ratios observed in carbon 1s photoelectron spectroscopy for a number of systems. $hv = 330$ eV.

System	Ratio	Measured
CCl_4/CH_4	CCl_4/CH_4	0.55
$CH_3C{\equiv}CCH_3$	$C{\equiv}/CH_3$	0.80
$CH_3C{\equiv}N$	CN/CH_3	0.94
$CH_3C{\equiv}CH$	C/CH_3	0.95
$CH_3C{\equiv}CH$	CH/CH_3	1.14
$CH_2{=}CHF$	CHF/CH_2	0.93
CH_3CH_2F	CH_2F/CH_3	0.88
CH_3CHF_2	CHF_2/CH_3	0.87
CH_3CF_3	CF_3/CH_3	0.74
$1,3,5-C_6H_3F_3$	CF/CH	0.88
$1,4-C_6H_4F_2$	CF/CH	0.87
$1,2,4,5-C_6H_2F_4$	CF/CH	0.92
CH_3CH_2Br	CH_2Br/CH_3	0.92
CH_3CHO	CHO/CH_3	1.00

It is apparent from these results that the intensity ratios often do not reflect the stoichiometry of the molecule. Although these effects are often associated with the presence of atoms from which there will be significant scattering, such as chlorine, there are also noticeable effects even with first-row elements such as carbon, nitrogen, oxygen. These effects must be taken into account in any attempt to use inner-shell photoelectron spectroscopy to obtain quantitative information.

4. Two-hole ionization energies

The ionization of an inner-shell electron leads to a positive charge being created at a particular site in a molecule. There are also a number of chemical processes that involve creation of a localized charge (either positive or negative). These include protonation (basicity), deprotonation (acidity), acid-catalyzed reactions, and electrophilic reactions. There are, therefore, many correlations between inner-shell ionization energies and the energies involved for these chemical processes. Understanding the factors that affect inner-shell ionization energies has helped to provide a better understanding of a number of chemical phenomena.

To a good approximation, the energy involved in creating a charge at a specific site in a molecule depends on two quantities. The first is the electrostatic potential in the original molecule at the site where the charge will be created. This can be represented as V, which is the potential energy that a unit positive charge would have at that site. The second is the effect of the polarization of the system in response to the added charge. The surrounding charges rearrange to screen the new charge leading to a lowering of the energy of the system. This effect is represented by R, for relaxation energy. Thus, for the the same atom in two different sites, we have

$$\Delta I_1(0) = \Delta V - \Delta R \tag{16}$$

where $I_1(0)$ is the single-electron ionization energy.

Measurements of ionization energies alone do not allow us to sort out the effects of both of ΔV and ΔR. Two sorts of additional information have been used for this purpose: deprotonation energies, A, and double ionization energies. The relevant energies for these are

$$\Delta A = -\Delta V - \Delta R \tag{17}$$
$$\Delta I_2(0) = 2\Delta V - 4\Delta R \tag{18}$$
$$\Delta I_1(1) \equiv \Delta I_2(0) - \Delta I_1(0) = \Delta V - 3\Delta R \tag{19}$$

where $I_2(0)$ is the double-electron ionization energy and $I_1(1)$ is the energy needed to remove a second electron from the already ionized molecule. (Derivations of eqs. 16-19 can be found in ref. [2].) If the experimental energies are known, then any pair of eqs. 16-19 can be used to determine the values of ΔV and ΔR, and many such investigations have been made [35]. Unfortunately the availability of values for A is quite limited and the major source of values of $I_2(0)$ and $I_1(1)$ has been core-core-core Auger spectroscopy, which is limited to elements beyond the first row of the periodic table. Recently, however, it has been demonstrated that it is possible to measure double ionizations directly, opening the possibility of measurements for first-row elements. This new capability has lead to a number of publications, both theoretical and experimental, on this subject.

A convenient way to display the relationships that are implicit in eqs. 16-19 is in a Wagner plot, where the second ionization energy, $I_1(1)$ is plotted against the first, $I_1(0)$. Fig. 8 shows such a plot for the results of theoretical calculations for fluorinated and chlorinated methanes ($CH_{4-n}X_n$, X=F,Cl, $n = 1 - 4$) and for 2,2-dimethylpropane ($C(CH_3)_4$) relative to methane [2].

On such a plot, loci of constant ΔR have slopes of 1, and those of constant ΔV have slopes of 3. Several of each of these are shown. These loci provide a convenient way to visualize the contributions of ΔV and ΔR to the ionization shifts. For instance, for the fluoromethanes (solid circles) all of the points
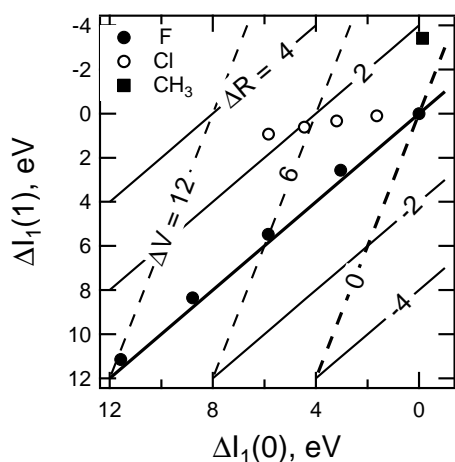
Figure 8: Wagner plot for fluoro- and chloromethanes and 2,2-dimethylpropane relative to methane. The solid lines show loci of constant ΔR and the dashed lines show loci of constant ΔV.

fall very close to the line for $\Delta R = 0$ but are displaced along it. From this we can see that relaxation effects play little role in determining the ionization-energy shifts for the fluoromethanes. These are determined almost entirely by the potential in the initial state and, hence, by the charge distribution in the neutral molecule. For the chloromethanes (open circles) it is apparent that relaxation effects play an important role. These increase with increasing numbers of chlorines, which are highly polarizible. ΔV is seen to be important for the chloromethanes, although less so than for the fluoromethanes, in keeping with the lower electronegativity of chlorine relative to fluorine. For 2,2-dimethylpropane, the overall shift in the carbon 1s ionization energy $\Delta I_1(0)$ is small, but this small number results from the near cancellation of the effect of ΔV by the effect of ΔR.

Wagner plots have been extensively used by Ueda and Takahashi [3] to illustrate the relative importance of initial-state and relaxation effects in the core-ionization of a variety of small molecules.

The foregoing discussion has dealt entirely with double-core-hole ionization with both holes on the same atom. It has recently become possible to measure double-core-hole ionization with the two holes on different atomic sites in the same molecule, and considerable theoretical effort has been put into exploring what new information might come out of such measurements [35]. A modified Wagner plot has been proposed as a useful way to display such results [2] and a number of such plots have been presented by Ueda and Takahashi [3].

The investigation of double-hole ionization is continuing to be a very active field [3, 36], and we can look forward to interesting new results to come from it.

5. Acknowledgments

[1] J. Söderström, N. Märtensson, O. Travnikova, M. Patanen, C. Miron, L. J. Sæthre, K. J. Børve, J. J. Rehr, J. J. Kas, F. D. Vila, T. D. Thomas, S. Svensson, Phys. Rev. Lett. 108 (2012) 193005.

[2] T. D. Thomas, J. Phys. Chem. A 116 (2012) 3856–3865.

[3] K. Ueda, O. Takahashi, J. Electr. Spectrosc. and Relat. Phenom. 185 (2012) 301–311. doi:10.1016/j.elspec.2012.04.003.

[4] It is not obvious *a priori* that the recoil energy will divide in this way especially for valence electrons, which are delocalized, and it is possible to imagine situations in which there would be no internal excitation. At this time, all of the experimental evidence for both core and valence electrons indicates that the picture described here is correct. Moreover, for photoemission of electrons at kinetic energies above about 10 eV, one can produce theoretical arguments that this picture is reasonable.

[5] W. Domcke, L. S. Cederbaum, J. Electr. Spectrosc. and Relat. Phenom. 13 (1978) 161–174.

[6] E. Kukk, K. Ueda, U. Hergenhahn, X.-J. Liu, G. Prümper, H. Yoshida, Y. Tamenori, C. Makochekanwa, T. Tanaka, M. Kitajima, H. Tanaka, Phys. Rev. Lett. 95 (2005) 133001.

[7] T. D. Thomas, E. Kukk, R. Sankari, H. Fukuzawa, G. Prümper, K. Ueda, R. Püttner, J. Harries, Y. Tamenori, T. Tanaka, M. Hoshino, H. Tanaka, J. Chem. Phys. 128 (2008) 144311.

[8] T. D. Thomas, E. Kukk, H. Fukuzawa, K. Ueda, R. Püttner, Y. Tamenori, T. Asahina, N. Kuze, H. Kato, M. Hoshino, H. Tanaka, M. Meyer, J. Plenge, A. Wirsing, E. Serdaroglu, R. Flesch, E. Rühl, Phys. Rev. A 79 (2009) 022506.

[9] E. Kukk, T. D. Thomas, K. Ueda, in: J. Phys: Conference Ser. vol. 194, 2009, p. 012007.

[10] T. D. Thomas, E. Kukk, T. Ouchi, A. Yamada, H. Fukuzawa, K. Ueda, R. Püttner, I. Higuchi, Y. Tamenori, T. Asahina, N. Kuze, H. Kato, M. Hoshino, H. Tanaka, A. Lindblad, L. J. Sæthre, J. Chem. Phys. 133 (2010) 174312.

[11] E. Kukk, T. D. Thomas, K. Ueda, J. Electr. Spectrosc. and Relat. Phenom. 183 (1-3) (2011) 53–58.

[12] Y.-P. Sun, C.-K. Wang, F. Gel'mukhanov, Phys. Rev. A 82 (2010) 052506.

[13] T. D. Thomas, E. Kukk, K. Ueda, T. Ouchi, K. Sakai, T. X. Carroll, C. Nicolas, O. Travnikova, C. Miron, Phys. Rev. Lett 106 (2011) 193009.

[14] The small effect of the difference between the moments-of-inertia of the neutral molecule and the ion has been ignored. See ref. [13].

[15] T. D. Thomas, E. Kukk, K. Ueda, T. Ouchi, K. Sakai, T. X. Carroll, C. Nicolas, O. Travnikova, C. Miron, PLEIADES/SOLEIL, unpublished (2010).

[16] Several approximations have been made in deriving eqs. 10 and 11: (1) The electron emission is isotropic in the molecular frame. (2) The difference between the moments of inertia of the neutral molecule and the ion can be ignored. (3) A term of order $\Delta E^2/5$ can be ignored. See ref. [13] for addiitonal details.

[17] E. D. Poliakoff, H. C. Choi, R. M. Rao, A. G. Mihill, S. Kakar, K. Wang, V. McKoy, J. Chem. Phys. 103 (5) (1995) 1773–1787.

[18] The term "Franck-Condon excitation" is used in its traditional sense to refer to the vibrational excitation that results from the geometric changes.

[19] T. Fujikawa, R. Suzuki, L. Köver, J. Electr. Spectrosc. and Relat. Phenom. 151 (2006) 170–177.

[20] T. X. Carroll, K. J. Børve, L. J. Sæthre, J. D. Bozek, E. Kukk, J. A. Hahne, T. D. Thomas, J. Chem. Phys. 116 (2002) 10221.

[21] M. Matsumoto, K. Ueda, E. Kukk, H. Yoshida, T. Tanaka, M. Kitajima, H. Tanaka, Y. Tamenori, K. Kuramoto, M. Eharaf, H. Nakatsuji, Chem. Phys. Lett. 417 (1-3) (2006) 89–93.

[22] E. Plésiat, P. Decleva, F. Martin, Phys. Chem. Chem. Phys 14 (2012) 10853–10871.

[23] Other versions of this trend line obtained by extending or contracting the range that has been fit or by eliminating outliers all have negative slopes.

[24] K. Ueda, X.-J. Liu, G. Prümper, T. Lischke, T. Tanaka, M. Hoshino, H. Tanaka, I. Minkov, V. Kimberg, F. Gel'mukhanov, Chem. Phys. 329 (2006) 329–337.

[25] F. Martin, P. Decleva, E. Plésiat, L. Argenti, D. Ayuso, M. Patanen, K. Kooser, C. Miron, K. Ueda, E. Kukk, T. D. Thomas, research in progress (2012).

[26] R. Püttner, M. N. Piancastelli, D. Ceolin, research in progress.

[27] H. M. Köppe, A. L. D. Kilcoyne, J. Feldhaus, A. M. Bradshaw, J. Electr. Spectrosc. and Relat. Phenom. 75 (1995) 97–108.

[28] M. Hoshino, K. Nakagawa, T. Tanaka, H. Tanaka, A. De Fanis, K. Wang, B. Zimmerman, V. McKoy, K. Ueda, J. Phys. B: At. Mol. Opt. Phys. 39 (2006) 3047–3055.

[29] R. R. Lucchese, J. Söderström, T. Tanaka, M. Hoshino, M. Kitajima, H. Tanaka, A. De Fanis, J. E. Rubensson, K. Ueda, Phys. Rev. A 76 (2007) 012506.

[30] H. C. Choi, R. M. Rao, A. G. Mihill, S. Kakar, E. D. Poliakoff, K. Wang, V. McKoy, Phys. Rev. Lett. 72 (1994) 44–47. doi:10.1103/PhysRevLett.72.44.

[31] H. D. Cohen, U. Fano, Phys. Rev. 150 (1966) 30–33.

[32] S. E. Canton, E. Plésiat, J. D. Bozek, B. S. Rude, F. Martin, Proc. Natl. Acad. Sci. U.S.A 108 (2011) 7302–7306.

[33] L. Argenti, T. D. Thomas, E. Plésiat, X.-J. Liu, C. Miron, T. Lischke, G. Prümper, N. Sakai, T. Ouchi, R. Püttner, V. Sekushin, T. Tanaka, M. Hoshino, H. Tanaka, P. Decleva, K. Ueda, F. Martin, New. J. Phys. 14 (2012) 033012.

[34] J. A. López-Dominguez, D. Hardy, A. Das, E. D. Poliakoff, A. Aguilar, R. R. Lucchese, J. Electr. Spectrosc. and Relat. Phenom. 185 (2012) 211–218.

[35] Refs. [2, 3] review much of the work on double-core holes that was published before early 2012.

[36] P. Salén, P. van der Meulen, H. T. Schmidt, R. D. Thomas, M. Larsson, R. Feifel, M. N. Piancastelli, L. Fang, B. Murphy, T. Osipov, N. Berrah, E. Kukk, K. Ueda, J. D. Bozek, C. Bostedt, S. Wada, R. Richter, V. Feyer, K. C. Prince, Phys. Rev. Lett. 108 (2012) 153003. doi:10.1103/PhysRevLett.108.153003.

[37] J. Söderström, N. Mårtensson, O. Travnikova, M. Patanen, C. Miron, L. J. Sæthre, K. J. Børve, T. D. Thomas, S. Svensson, PLEIADES, SOLEIL, unpublished (2011).